Supporting Information

Shaping Single-crystalline Trimetallic Pt−Pd−Rh Nanocrystals toward High-efficiency C−C Splitting of Ethanol in Conversion to CO_2

Wei Zhu,[†,‡] Jun Ke,[†,‡] Si-Bo Wang,[†] Jie Ren,[§] Hong-Hui Wang,[§] Zhi-You Zhou,[§,*] Rui Si,[ᵠ] Ya-Wen Zhang,[†,*] and Chun-Hua Yan[†,*]

[†] Beijing National Laboratory for Molecular Sciences, State Key Laboratory of Rare Earth Materials Chemistry and Applications, PKU-HKU Joint Laboratory in Rare Earth Materials and Bioinorganic Chemistry, College of Chemistry and Molecular Engineering, Peking University, Beijing 100871, China.

[§] State Key Laboratory of Physical Chemistry of Solid Surfaces, Department of Chemistry, College of Chemistry and Chemical Engineering, Xiamen University, Xiamen 361005, China.

[ᵠ] Shanghai Synchrotron Radiation Facility, Shanghai Institute of Applied Physics, Chinese Academy of Sciences, Shanghai 201204, China.

* Correspondence to: ywzhang@pku.edu.cn, zhouzy@xmu.edu.cn, yan@pku.edu.cn.

[‡] These authors contributed equally to this work.

Supplementary Data

Table S1. DFT calculations on the reaction energies of possible reaction paths in EOR on alloyed Pt−Pd−Rh (111) and (100) planes of varied compositions.

Composition Pt:Pd:Rh	ΔE(I)[a]		ΔE(II)[b]		ΔE(III)[c]	
	(100) / eV	(111) / eV	(100) / eV	(111) / eV	(100) / eV	(111) / eV
1:0:0	1.13	1.45	−0.76	−0.77	4.27	3.36
0:1:0	1.61	1.42	−0.47	−0.40	3.70	3.05
0:0:1	0.71	1.22	−1.03	−0.90	4.58	3.78
7:1:1	0.68	1.25	−1.05	−1.07	4.22	3.10
1:7:1	0.29	0.31	−1.30	−1.28	4.02	3.46
1:1:7	0.80	1.16	−1.10	−0.86	4.22	3.17
5:2:2	0.73	1.01	−0.96	−1.14	4.34	3.51
2:5:2	−0.10	0.39	−0.84	−1.24	4.54	3.91
2:2:5	0.72	0.00	−0.99	−1.00	4.56	3.32
4:4:1	−0.18	0.83	−1.14	−1.20	4.53	3.29
4:1:4	0.08	1.54	−1.10	−1.12	4.33	3.21
1:4:4	0.34	0.44	−0.68	−1.18	4.37	3.79
1:1:1	0.44	0.31	−1.03	−1.21	4.06	3.83

[a] $CH_2CH_2O_{(ad)} = CH_{2\,(ad)} + CH_2O_{(ad)}$

$\Delta E(\mathrm{I}) = E(\text{metal with } CH_2) + E(\text{metal with } CH_2O) - E(\text{metal with } CH_2CH_2O) - E(\text{metal})$

[b] $CHCO_{(ad)} = CH_{(ad)} + CO_{(ad)}$

$\Delta E(\mathrm{II}) = E(\text{metal with CH}) + E(\text{metal with CO}) - E(\text{metal with CHCO}) - E(\text{metal})$

[c] $CO_{(ad)} + OH_{(ad)} = CO_{2\,(g)} + H^+ + e^-$

$\Delta E(\mathrm{III}) = E(\text{metal}) \times 2 + E(CO_2) + E(\mathrm{H}) - E(\text{metal with CO}) - E(\text{metal with OH})$

Note: Replacing H^+ (aq) with isolated H atom would not change the variation sequence.

Table S2. Pt:Pd:Rh ratios of the as-synthesized shaped Pt−Pd−Rh nanocrystals obtained from ICP-AES and XPS analyses.

Sample	Atomic ratio of elements (Pt:Pd:Rh)	
	ICP-AES	[a]XPS
Pt_3PdRh NCs	71:20:9	34:11:55
PtPdRh NCs	37:37:26	7:10:83
PtPdRh NCs-200	36:35:29 (18.5 nm) - -	10:25:65 (18.5 nm) 15:25:60 (13.8 nm) 27:29:44 (8.8 nm)
PtPdRh NTOs	39:33:28	28:14:58
Pt_3PdRh NTOs	62:20:18	70:16:14
$PtPd_3Rh$ NTOs	21:63:16	13:56:31

[a] Background excluding, curve fitting, and peak area integration were performed using CasaXPS v2.3.15 software. Amounts of Pt, Pd and Rh were obtained from the peak area (*A*) of Pt 4f, Pd 3d, and Rh 3d spectra. The inelastic mean free path was estimated to be 16−20 Å from Ref. S1 ($h\nu$ = 1486.6 eV, kinetic energy = ~1150−1415 eV). The atomic ratio of the three elements at surface levels was calculated through the following equation:

$$\mathrm{Pt:Pd:Rh} = \frac{A(\mathrm{Pt})}{S(\mathrm{Pt})} : \frac{A(\mathrm{Pd})}{S(\mathrm{Pd})} : \frac{A(\mathrm{Rh})}{S(\mathrm{Rh})}$$

wherein, *S* is the relative sensitivity factor. Uncertainty for the fitting and measurements was estimated to be about ±30%.

Table S3. Detailed EXAFS Parameters of Shaped Pt−Pd−Rh Nanocrystals.[a]

Sample	Edge	Shell	CN	R / Å	σ^2 / Å^{-2}	E_0 / eV
PtPdRh NCs	Pt L_3	Pt−Pt	7.5 ±0.5	2.746 ±0.003	0.004 ±0.001	7.4 ±0.5
		Pt−Pd	2.5 ±0.3	2.739 ±0.005	0.003 ±0.001	
	Pd K	Pd−Pd	7.0 ±0.5	2.733 ±0.003	0.004 ±0.001	−2.1 ±0.4
		Pd−Pt	2.5 ±0.3	2.739 ±0.005	0.003 ±0.001	
	Rh K	Rh−Rh	8.3 ±0.4	2.689 ±0.002	0.004 ±0.001	−0.5 ±0.3
PtPdRh NTOs	Pt L_3	Pt−Pt	4.6 ±0.5	2.728 ±0.007	0.003 ±0.001	7.0 ±0.5
		Pt−Pd	1.2 ±0.7	2.74 ±0.02	0.001 ±0.002	
		Pt−Rh	3.3 ±0.5	2.701 ±0.008	0.005 ±0.002	
	Pd K	Pd−Pd	8.0 ±1.3	2.741 ±0.009	0.004 ±0.001	−1.7 ±0.9
		Pd−Pt	1.2 ±0.7	2.74 ±0.02	0.001 ±0.002	
	Rh K	Rh−Rh	4.4 ±0.3	2.694 ±0.005	0.004 ±0.001	−1.3 ±0.5
		Rh−Pt	3.3 ±0.5	2.701 ±0.008	0.004 ±0.001	

[a] CN, coordination number; R, interatomic distance between absorber and backscatter atoms; σ^2, Debye−Waller-type factor; ΔE_0, difference between the zero kinetic energy of the sample. S_0^2 was defined as 0.82 for Pt, 0.78 for Pd, and 0.89 for Rh from standard samples.

Table S4. Reduction peak potentials of oxides on Pt−Pd−Rh trimetallic nanocrystals from CV measurements in 0.1 M $HClO_4$ solution. The initial ones were obtained from the 5^{th} cycles of CV measurements of as-obtained samples, and the stable ones were obtained from the 10^{th} cycles of CV measurements in 0.1 M $HClO_4$ solution after EOR LSVs tests.

Sample	Initial peak potential / V	Stable peak potential / V
PtPdRh NCs	0.48	0.52
Pt_3PdRh NCs	0.47	0.72
PtPdRh NCs-200	0.47	0.57
PtPdRh NTOs	0.44	0.53
Pt_3PdRh NTOs	0.48	0.68
$PtPd_3$Rh NTOs	0.41	0.56

Table S5. Pt:Pd:Rh ratios of shaped Pt−Pd−Rh nanocrystals after electro-chemical tests measured by EDS analysis.

Sample	Atomic ratio of elements (Pt:Pd:Rh)
PtPdRh NCs	44:35:21
Pt_3PdRh NCs	81:15:4
PtPdRh NTOs	37:36:27
Pt_3PdRh NTOs	79:19:2
$PtPd_3$Rh NTOs	20:70:10

Table S6. Summary of current densities at various potential extracted from LSVs measurements of all nanocatalysts in 0.5 M CH_3CH_2OH / 0.1 M $HClO_4$ solution

Sample	ECSA / cm^2	$J_{0.45\ V}$ / $mA.cm^{-2}$	$J_{0.5\ V}$ / $mA.cm^{-2}$	$J_{0.6\ V}$ / $mA.cm^{-2}$	$J_{0.7\ V}$ / $mA.cm^{-2}$
Pt Black	1.60	4.19×10^{-3}	9.30×10^{-3}	4.42×10^{-2}	1.09×10^{-1}
Pd/C	1.92	~0	1.15×10^{-4}	4.81×10^{-4}	9.22×10^{-4}
Rh NCs	2.17	5.81×10^{-3}	1.22×10^{-2}	2.97×10^{-2}	1.56×10^{-2}
PtRh NCs	0.48	1.26×10^{-3}	6.61×10^{-3}	4.25×10^{-2}	1.70×10^{-1}
PtPd NCs	8.96	4.14×10^{-3}	1.05×10^{-2}	4.44×10^{-2}	9.78×10^{-2}
Pt_3PdRh NCs	2.00	5.92×10^{-3}	1.69×10^{-2}	8.65×10^{-2}	2.00×10^{-1}
PtPdRh NCs	0.19	~0	~0	7.95×10^{-3}	6.26×10^{-2}
8.8 nm PtPdRh NCs-200	0.31	1.18×10^{-2}	4.60×10^{-2}	2.36×10^{-1}	5.02×10^{-1}
13.8 nm PtPdRh NCs-200	0.35	5.76×10^{-3}	3.08×10^{-2}	1.50×10^{-1}	3.30×10^{-1}
18.5 nm PtPdRh NCs-200	5.76	3.32×10^{-3}	8.83×10^{-3}	4.64×10^{-2}	1.31×10^{-1}
PtPdRh NTOs	1.73	1.07×10^{-2}	4.47×10^{-2}	1.43×10^{-1}	3.20×10^{-1}
Pt_3PdRh NTOs	0.32	1.40×10^{-2}	4.91×10^{-2}	2.19×10^{-1}	4.53×10^{-1}
$PtPd_3Rh$ NTOs	0.51	2.05×10^{-3}	8.96×10^{-3}	6.36×10^{-2}	1.82×10^{-1}
PtRh(Sn)/SnO_2 NPs	1.75	4.24×10^{-3}	1.57×10^{-2}	5.71×10^{-2}	1.11×10^{-1}
niggliite PtRhSn/C NPs	0.37	6.17×10^{-2}	8.20×10^{-2}	1.23×10^{-1}	1.84×10^{-1}

Table S7. Mass activity of nanocatalysts at 0.5 V from LSVs measurements in 0.5 M CH_3CH_2OH / 0.1 M $HClO_4$ solution. The concentrations of Pt and noble metals colloidal solution used in the electrochemical tests were determined by ICP-AES.

Sample	ECSA / mg_{Pt} (cm^2 mg^{-1})	ECSA / mg_{metal} (cm^2 mg^{-1})	$J_{500\ mV}$ (mA mg_{Pt}^{-1})	$J_{500\ mV}$ (mA mg_{metal}^{-1})
Pt Black	176.6	176.6	1.64	1.64
Rh NCs	/	89.8	/	0.52
Pt_3PdRh NCs	134.0	108.5	2.27	1.83
8.8 nm PtPdRh NCs-200	65.8	33.9	0.78	0.40
13.8 nm PtPdRh NCs-200	47.6	26.5	0.28	0.15
PtPdRh NTOs	344.3	173.3	3.68	1.85
Pt_3PdRh NTOs	221.6	170.0	3.10	2.38

Table S8. Summary of current densities gained from chronoamperometric experiments recorded at 0.5 V and 0.7 V *vs.* NHE of all nanocatalysts in 0.5 M CH_3CH_2OH / 0.1 M $HClO_4$ solution

Sample	$J_{initial\ at\ 0.5\ V}$ / mA.cm^{-2}	$J_{1h\ at\ 0.5\ V}$ / mA.cm^{-2}	$J_{5h\ at\ 0.7\ V}$ / mA.cm^{-2}
Pt Black	3.51×10^{-2}	1.46×10^{-2}	3.75×10^{-2}
Rh NCs	3.31×10^{-2}	1.74×10^{-3}	~0
PtRh NCs	3.82×10^{-2}	5.46×10^{-3}	~0
PtPd NCs	1.65×10^{-2}	6.69×10^{-3}	6.39×10^{-3}
Pt_3PdRh NCs	5.15×10^{-2}	1.32×10^{-2}	8.17×10^{-3}
8.8 nm PtPdRh NCs-200	9.93×10^{-2}	2.63×10^{-2}	1.74×10^{-2}
13.8 nm PtPdRh NCs-200	6.22×10^{-2}	1.76×10^{-2}	4.36×10^{-3}
PtPdRh NTOs	5.27×10^{-2}	3.05×10^{-3}	2.18×10^{-3}
Pt_3PdRh NTOs	8.67×10^{-2}	6.13×10^{-3}	6.01×10^{-3}
$PtPd_3Rh$ NTOs	2.01×10^{-2}	~0	~0
niggliite PtRhSn/C NPs	3.66×10^{-2}	8.06×10^{-3}	9.11×10^{-3}

Table S9. Assignments of the possible characteristic adsorption bands in ethanol electro-oxidation reaction.

Band Position	Reported Position	Assignment
1050 cm^{-1}	1050 cm^{-1} (Ref. S4)	C−O stretching vibration of ethanol
1111 cm^{-1}	1108 cm^{-1} (Ref. S3)	Cl−O stretching vibration of ClO_4^-
1285 cm^{-1}	1280 cm^{-1} (Ref. S2)	Characteristic absorption of C−O stretching in acetic acid
1350-1370 cm^{-1}	1368 cm^{-1} (Ref. S4)	C-H stretching of CH_3COOH
1715 cm^{-1}	1705 cm^{-1} (Ref. S2)	C=O stretching vibration of CH_3CHO and CH_3COOH
1830 cm^{-1}	1800-1840 cm^{-1} (Ref. S2)	stretching vibration of bridge adsorbed CO
2030 cm^{-1}	2030-2065 cm^{-1} (Ref. S2)	stretching vibration of linear adsorbed CO
2340 cm^{-1}	2343 cm^{-1} (Ref. S3)	O=C=O asymmetric stretch vibration of CO_2

Table S10. Summaries of adsorption band intensities of *in situ* FTIR performed at 0.65 V and 0.95 V on shaped Pt−Pd−Rh nanocrystals in 0.1 M $HClO_4$ / 0.5 M CH_3CH_2OH solution at 2340 cm^{-1} and 1285 cm^{-1}.

Sample	Band intensities				Ratio of band intensities (2340 cm^{-1} / 1285 cm^{-1})	
	2340 cm^{-1} (0.65 V)	2340 cm^{-1} (0.95 V)	1285 cm^{-1} (0.65 V)	1285 cm^{-1} (0.95 V)	0.65 V	0.95 V
Pt Black	6.9×10^{-4}	3.1×10^{-3}	3.9×10^{-4}	3.3×10^{-3}	1.8	0.9
Pt-Pd NCs	3.6×10^{-4}	1.8×10^{-3}	1.5×10^{-4}	2.0×10^{-3}	2.3	0.9
Pt-Rh NCs	1.6×10^{-4}	1.1×10^{-3}	1.8×10^{-4}	1.4×10^{-3}	0.9	0.8
PtPdRh NCs	5.5×10^{-4}	1.9×10^{-3}	4.2×10^{-4}	2.5×10^{-3}	1.3	0.8
Pt_3PdRh NCs	7.4×10^{-4}	3.8×10^{-3}	6.1×10^{-4}	6.2×10^{-3}	1.2	0.6
PtPdRh NTOs	3.6×10^{-3}	8.9×10^{-3}	3.1×10^{-4}	6.7×10^{-3}	11	1.3
Pt_3PdRh NTOs	5.7×10^{-4}	2.5×10^{-3}	2.5×10^{-4}	3.1×10^{-3}	2.2	0.8
$PtPd_3$Rh NTOs	8.0×10^{-5}	1.1×10^{-3}	8.3×10^{-5}	1.4×10^{-3}	1.0	0.8
PtPdRh NCs-200	1.7×10^{-4}	8.2×10^{-4}	2.6×10^{-5}	8.0×10^{-4}	6.5	1.0

[a] $\Delta R/R(E_s^i) = (R(E_s^i) - R(E_R)) / R(E_R)$

$R(E_R)$ and $R(E_S^i)$ were the spectrum at reference potential and tested potential, respectively. (Ref. S5)

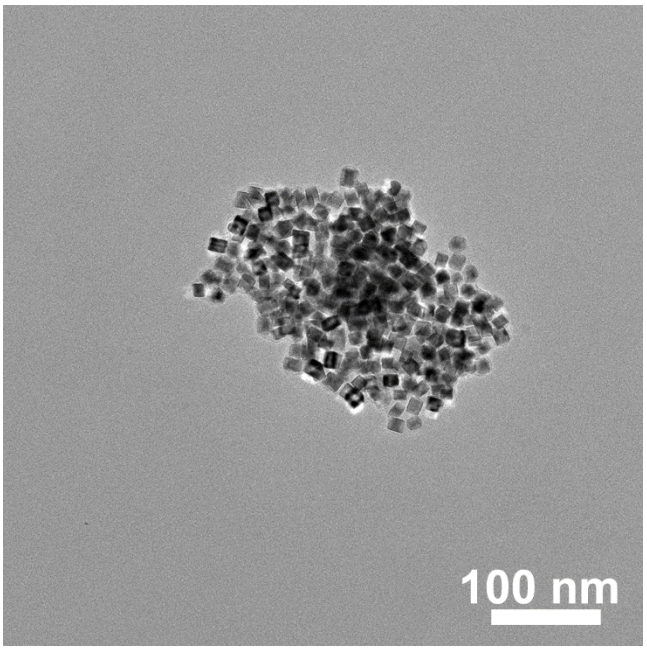

Figure S1. TEM image of PtPdRh NCs after 12 hours' UV/ozone irradiation.

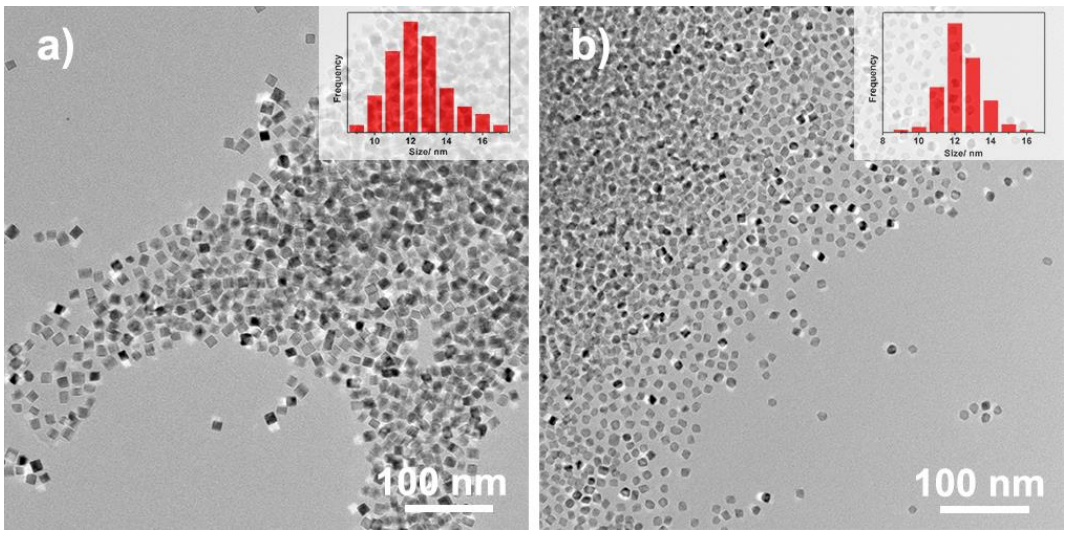

Figure S2. TEM images of a) PtPdRh NCs and b) PtPdRh NTOs. The insets are the size distribution histograms of nanocrystals.

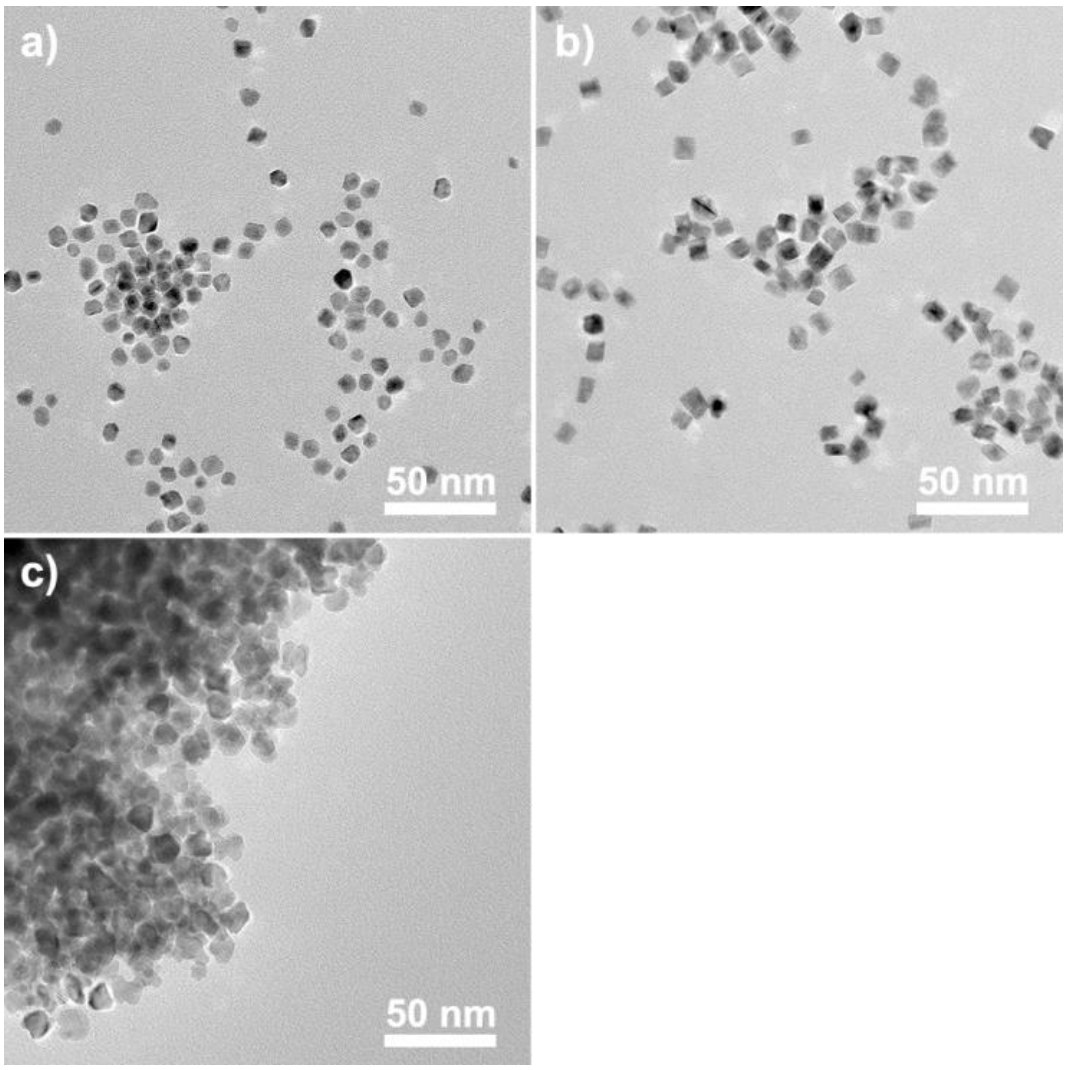

Figure S3. TEM images of PtPdRh nanocrystals synthesized by adjusting the concentrations of bromide and iodide ions: a) absence of KI and KBr; b) absence of KBr, and 0.006 mmol KI; c) absence of KI, and 6 mmol KBr. The other synthetic parameters were as follows: 0.02 mmol of H_2PtCl_6, 0.02 mmol of $RhCl_3$, 0.02 mmol of Na_2PdCl_4, 0.050 mmol HCl, 100 mg of PVP, 15 mL of total volume (diluted by deionized water), 180 ℃, 4 h. The results demonstrated that iodine ion mainly served as the shape controlled agent for the formation of cubic morphology, and bromide ion acted as an auxiliary to perfect the shape of nanocubes.

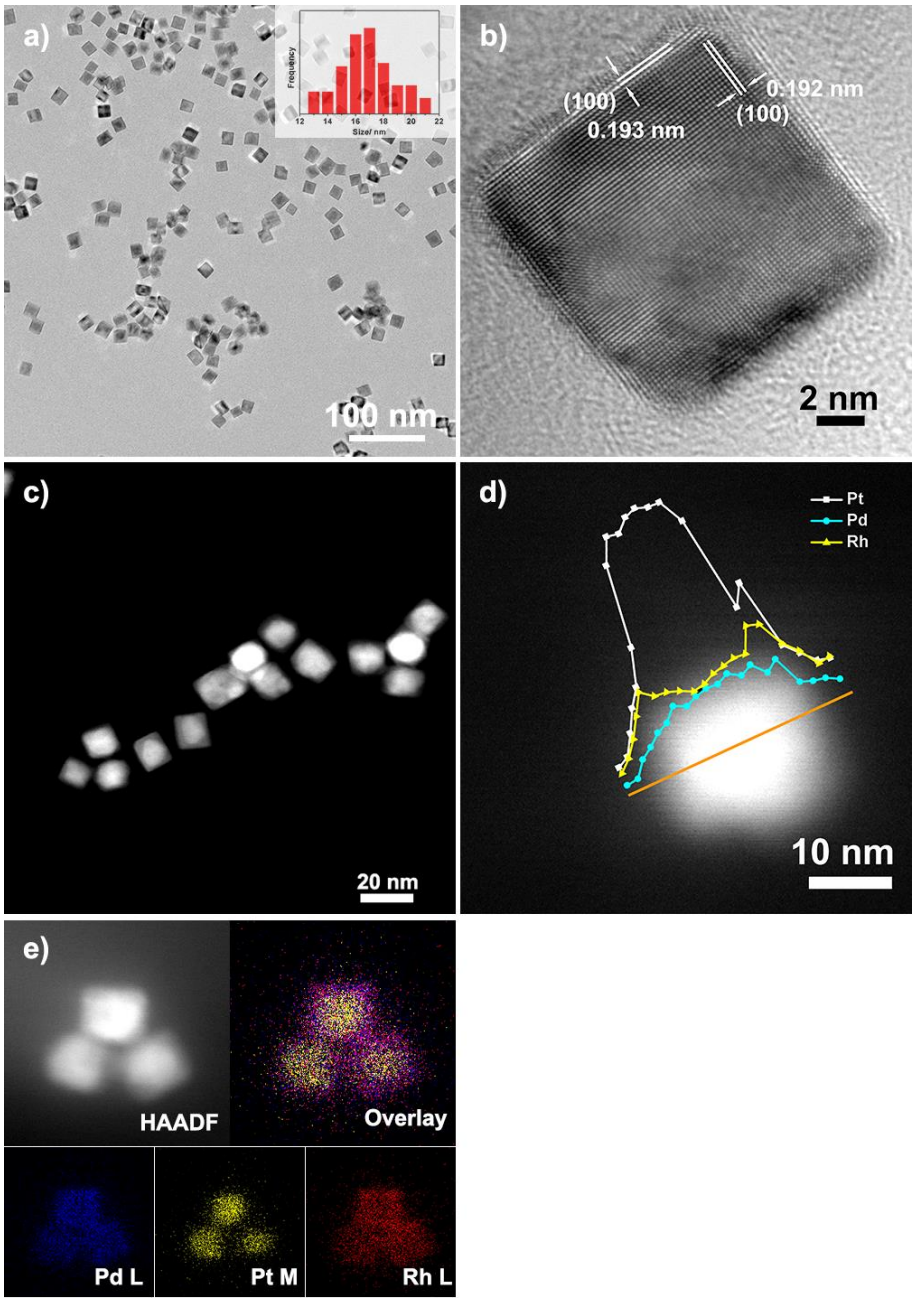

Figure S4. a) TEM image, b) HRTEM image, c) HAADF-STEM, d) HAADF-STEM EDS line scan profile, and e) HAADF-STEM EDS elemental mapping images of Pt_3PdRh NCs.

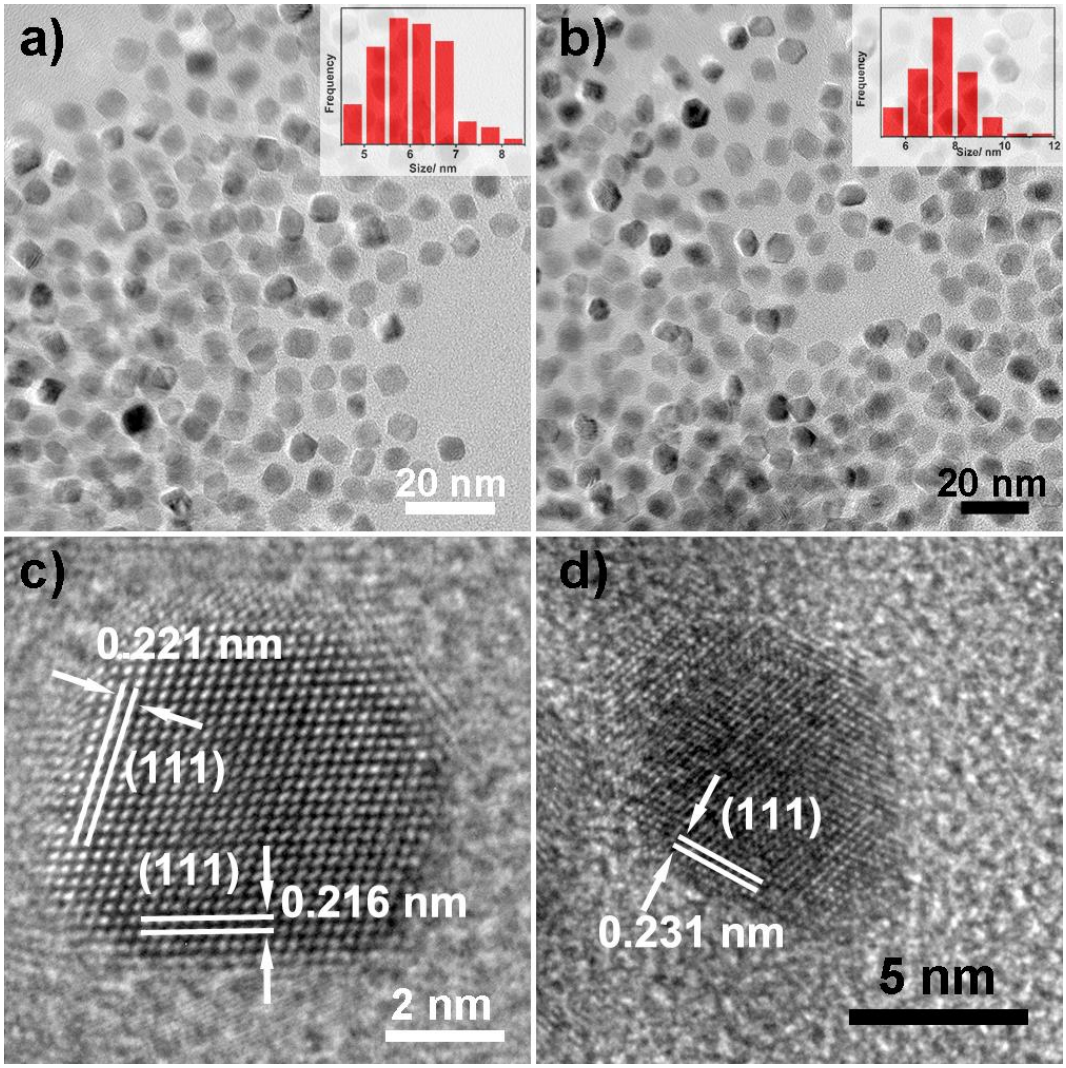

Figure S5. TEM images of a) Pt_3PdRh NTOs and b) $PtPd_3Rh$ NTOs (the insets are the corresponding size distribution histograms), HRTEM images of c) Pt_3PdRh NTOs and d) $PtPd_3Rh$ NTOs.

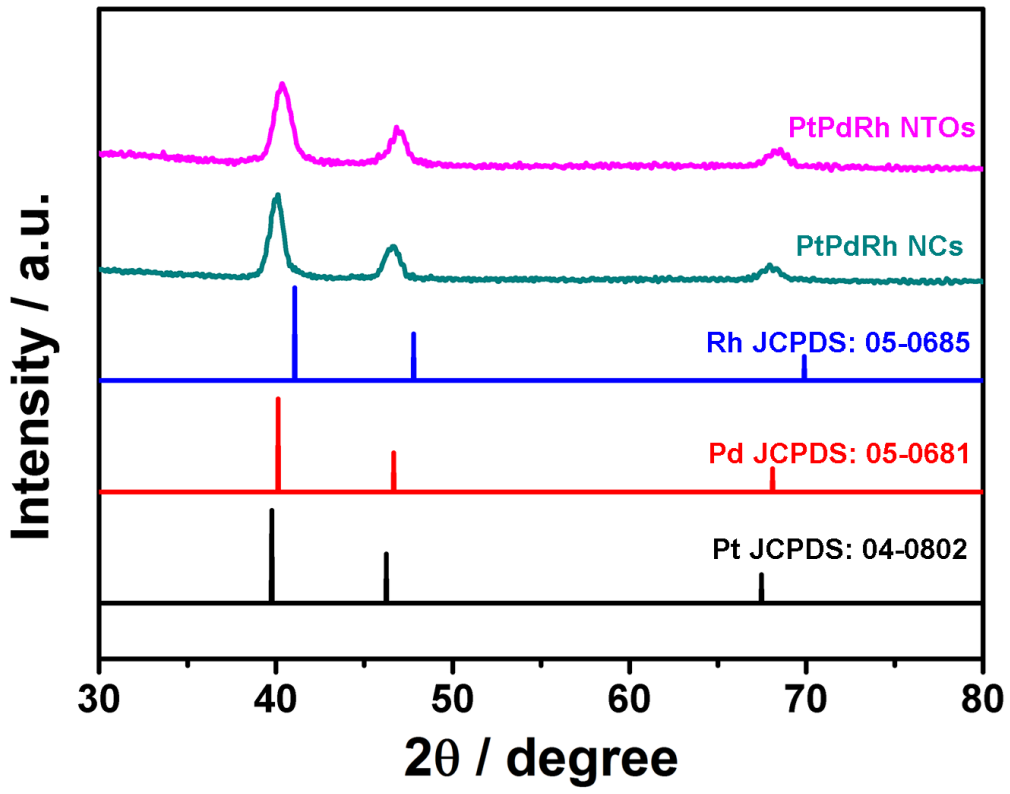

Figure S6. PXRD patterns of shaped Pt−Pd−Rh nanocrystals.

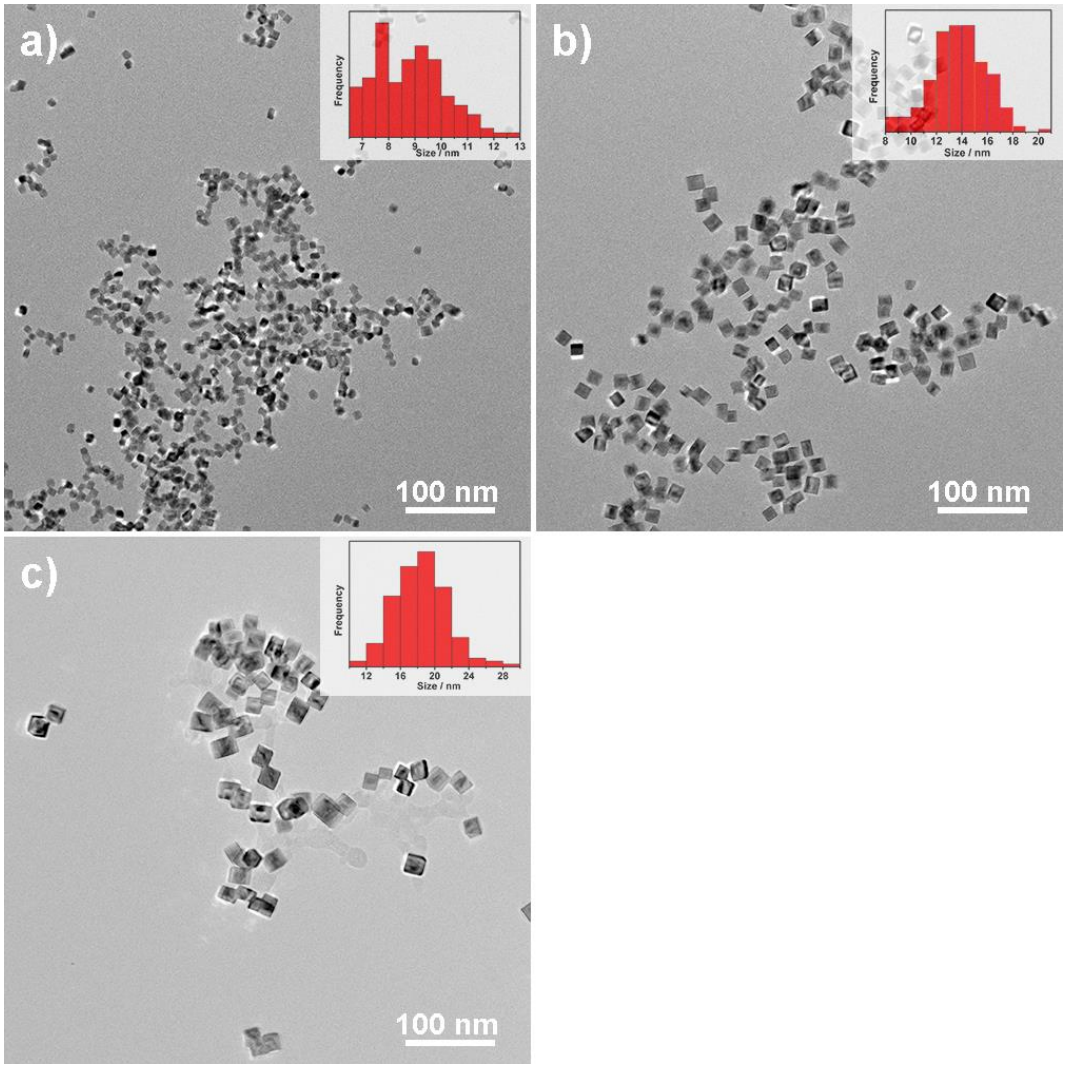

Figure S7. TEM images of a) 8.8 nm PtPdRh NCs-200, b) 13.8 nm PtPdRh NCs-200, and c) 18.5 nm PtPdRh NCs-200.

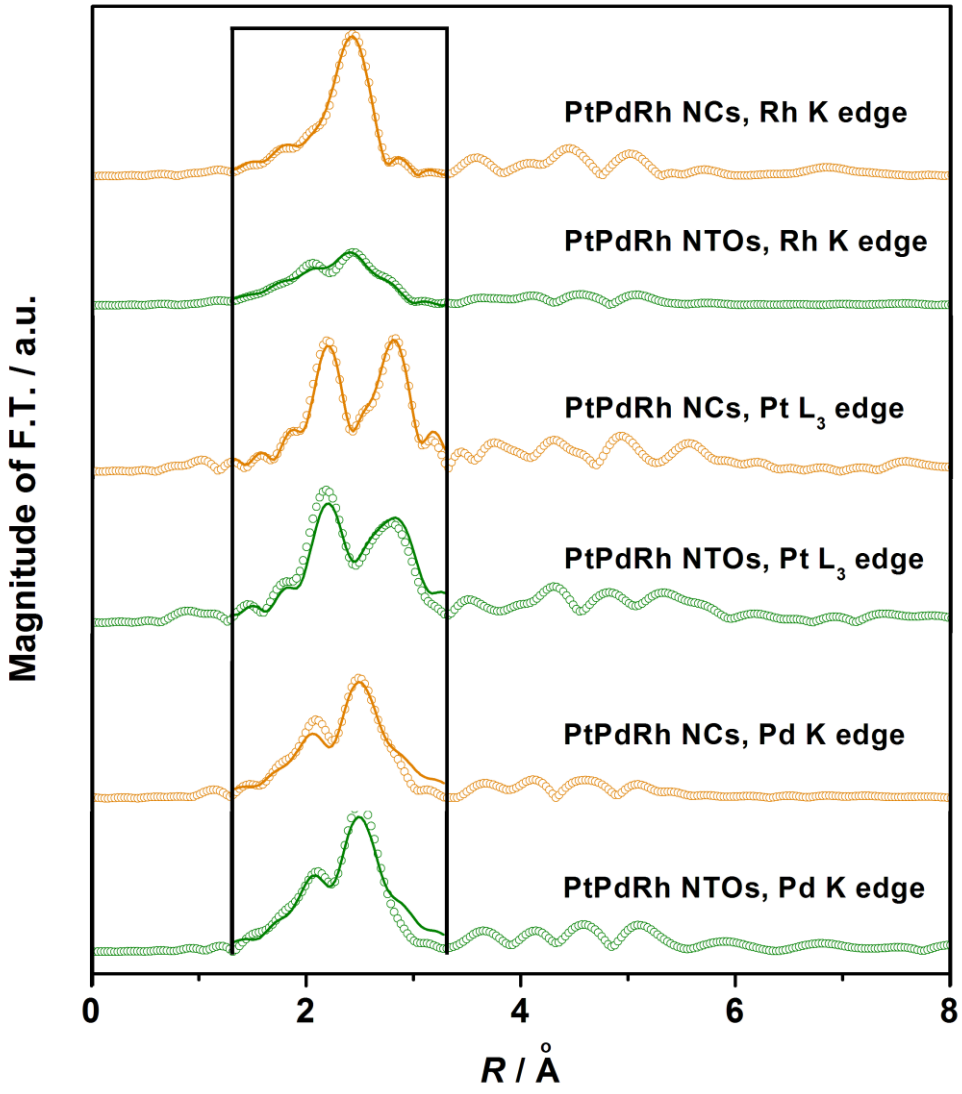

Figure S8. Fourier transforms of EXAFS spectra of PtPdRh NCs and PtPdRh NTOs. The dots are the experimental data, and the solid lines in the windows represent the corresponding fitting data.

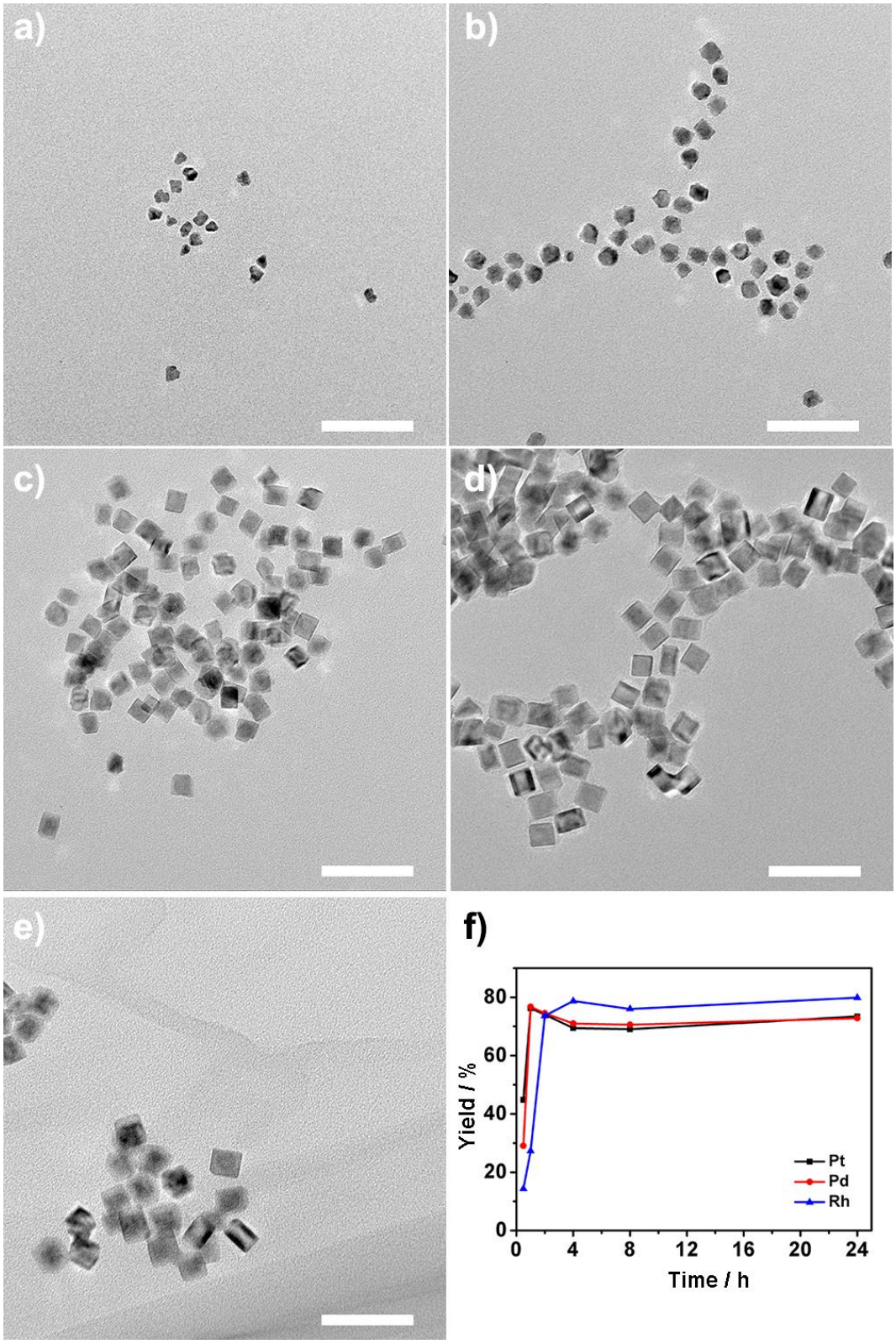

Figure S9. TEM images of Pt−Pd−Rh nanocrystals obtained from varied reaction time of synthesis: a) 0.5 h, b) 1.5 h, c) 2 h, d) 8 h, e) 24 h. The other conditions were the same as those in the synthesis of PtPdRh NCs. f) Yields of each element (ratio of the amount of each element in nanoparticles to its total amount) in the Pt−Pd−Rh nanocrystals synthesized at different times. The yields are converted from ICP-AES results of the as-obtained nanocrystals. Due to the loss in the washing procedure, the translated yields are smaller than the actual values. The scale bar in each TEM image is 50 nm.

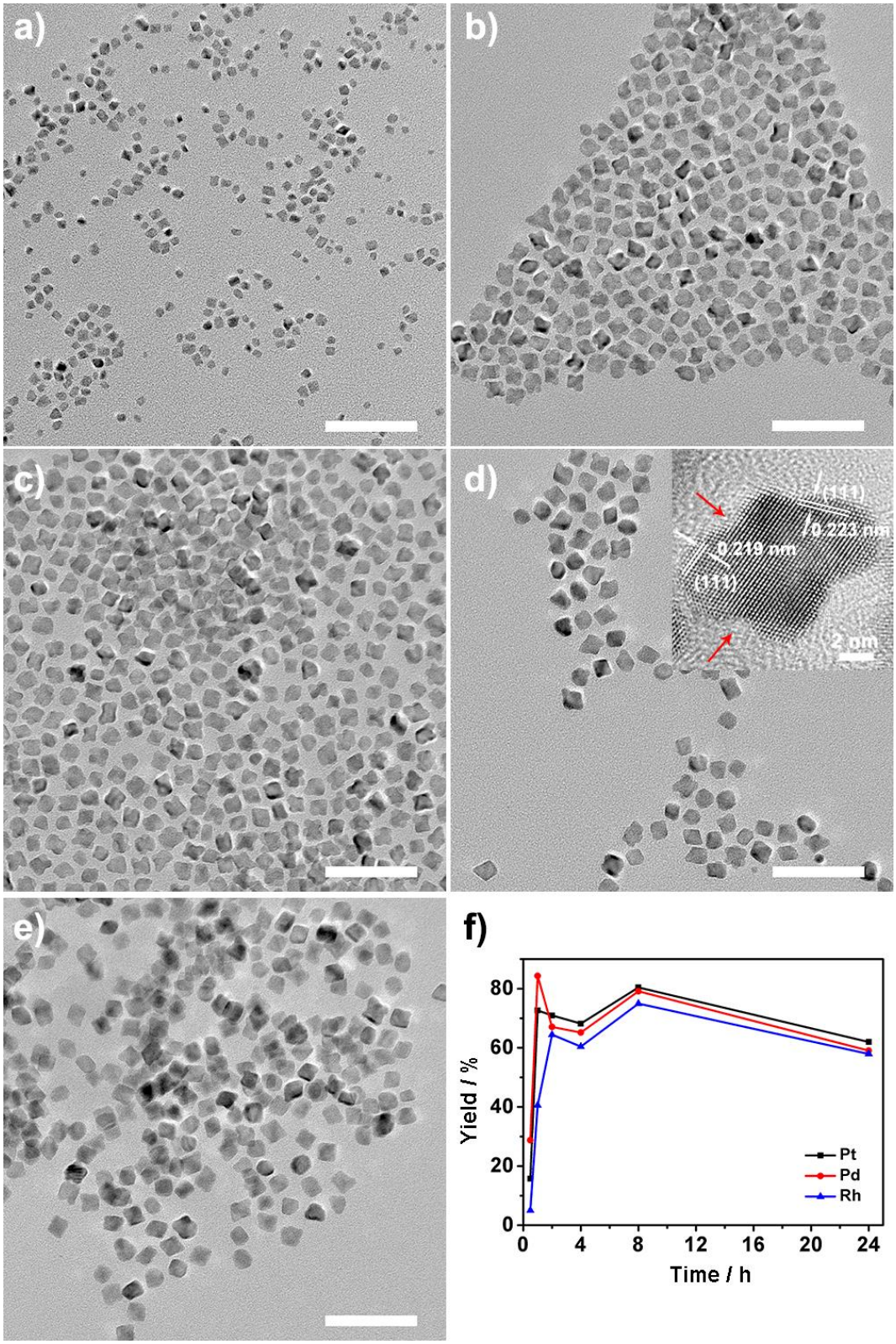

Figure S10. TEM images of Pt−Pd−Rh nanocrystals obtained from varied reaction time of synthesis: a) 0.5 h, b) 1.5 h, c) 2 h, d) 4 h, e) 24 h. The other conditions were the same as those in the synthesis of PtPdRh NTOs. f) Yields of each element (ratio of the amount of each element in nanoparticles to its total amount) in the Pt−Pd−Rh nanocrystals synthesized at different times. The yields are converted from ICP-AES results of the as-obtained nanocrystals. Due to the loss in the washing procedure, the translated yields are smaller than the actual values. The inset plane in panel d) was the corresponding HRTEM image of defective intermediates. The red arrows showed the sites where the surface recovery took place. The scale bar in each TEM image is 50 nm.

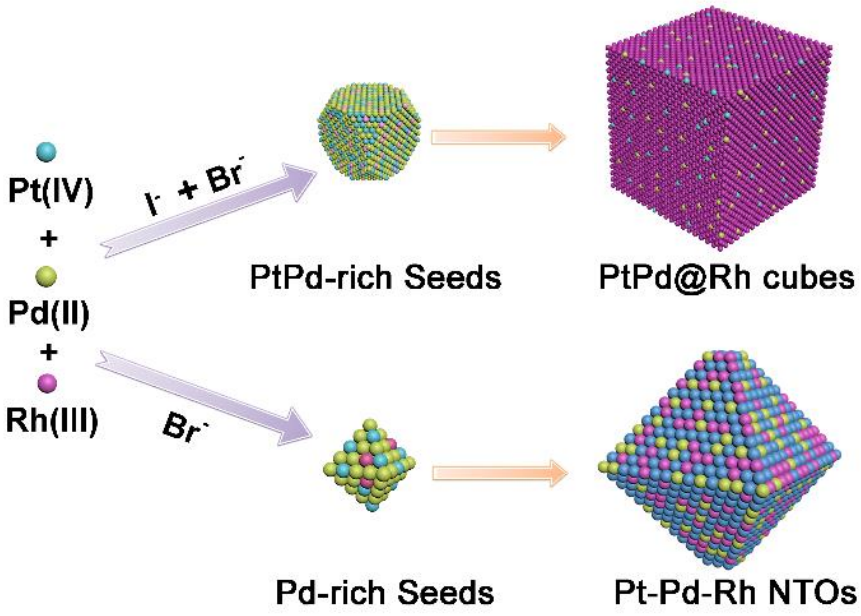

Figure S11. Growth mechanism of Pt−Pd−Rh NCs and Pt−Pd−Rh NTOs with distinct elemental distribution status.

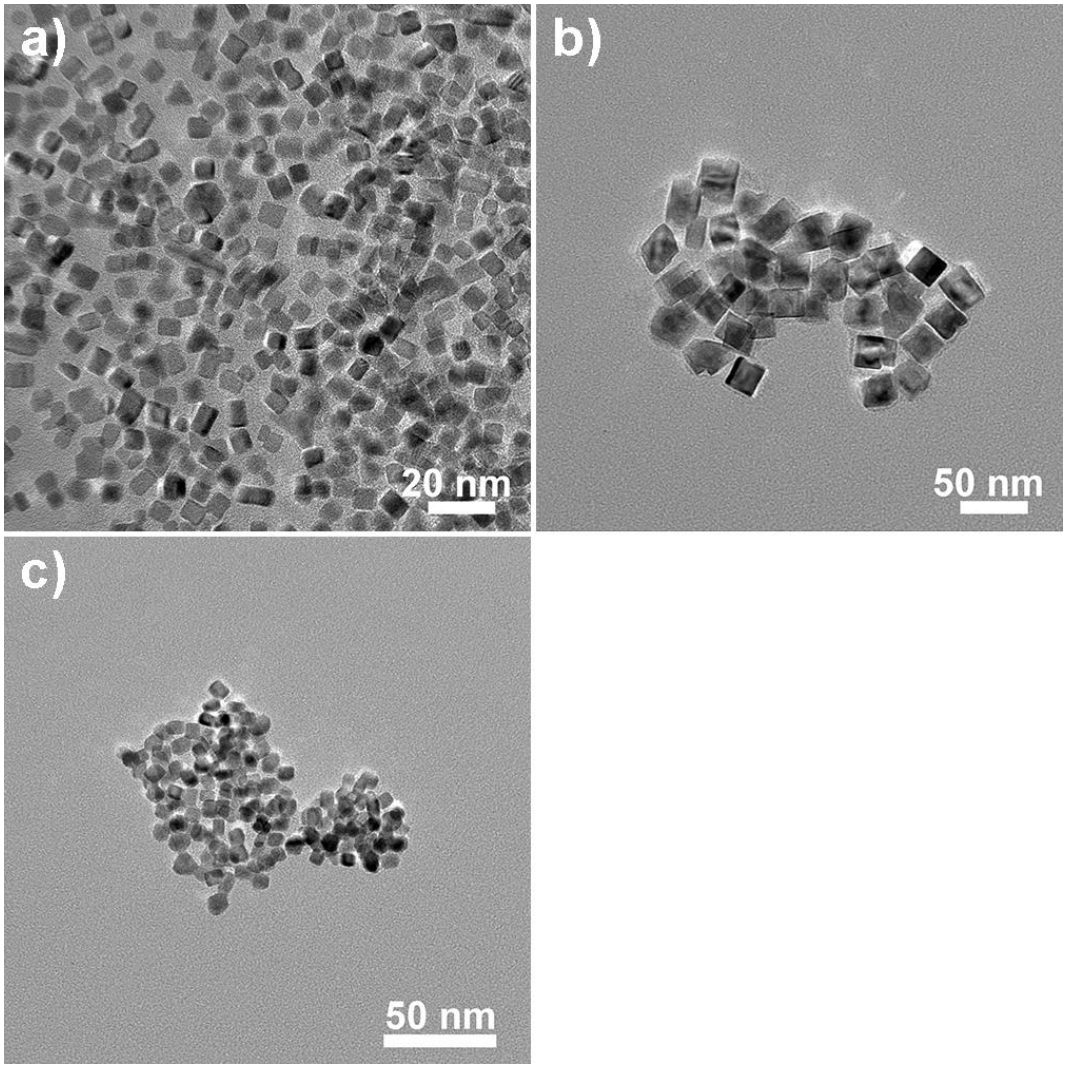

Figure S12. TEM images of a) Rh NCs, b) PtRh NCs, and c) PtPd NCs.

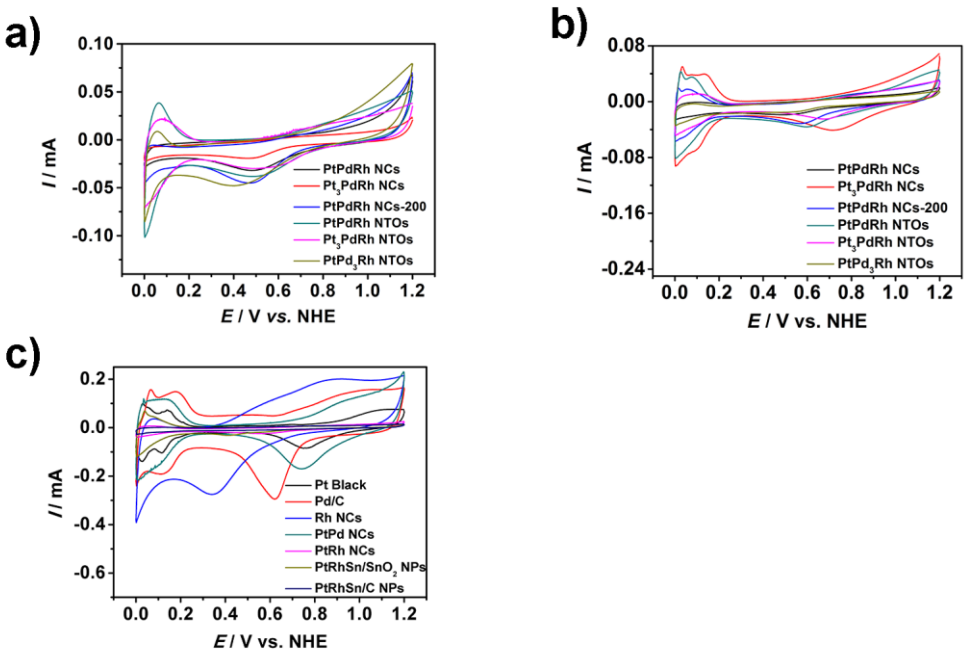

Figure S13. a) The 5th cycle of CV curves of shaped Pt−Pd−Rh NPs in 0.1 M $HClO_4$ solution, b) stable CV curves of shaped Pt−Pd−Rh NPs in 0.1 M $HClO_4$ solution, and c) stable CV curves of other catalysts in 0.1 M $HClO_4$.

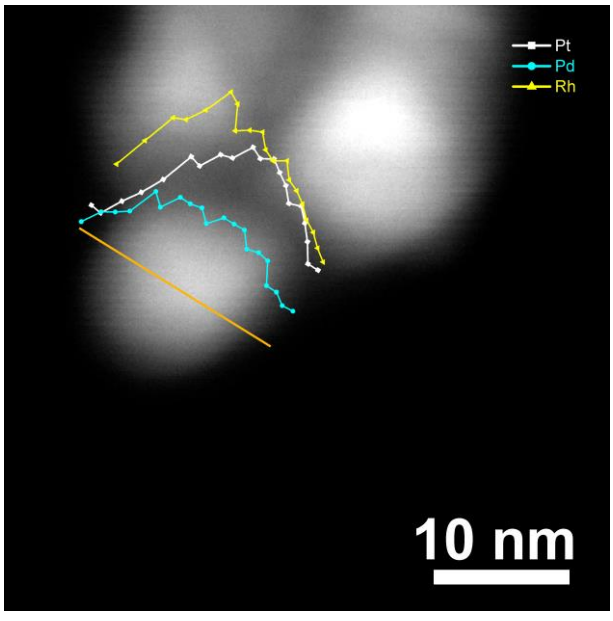

Figure S14. HAADF-STEM EDS line scan profile of PtPdRh NCs after catalysis reactions.

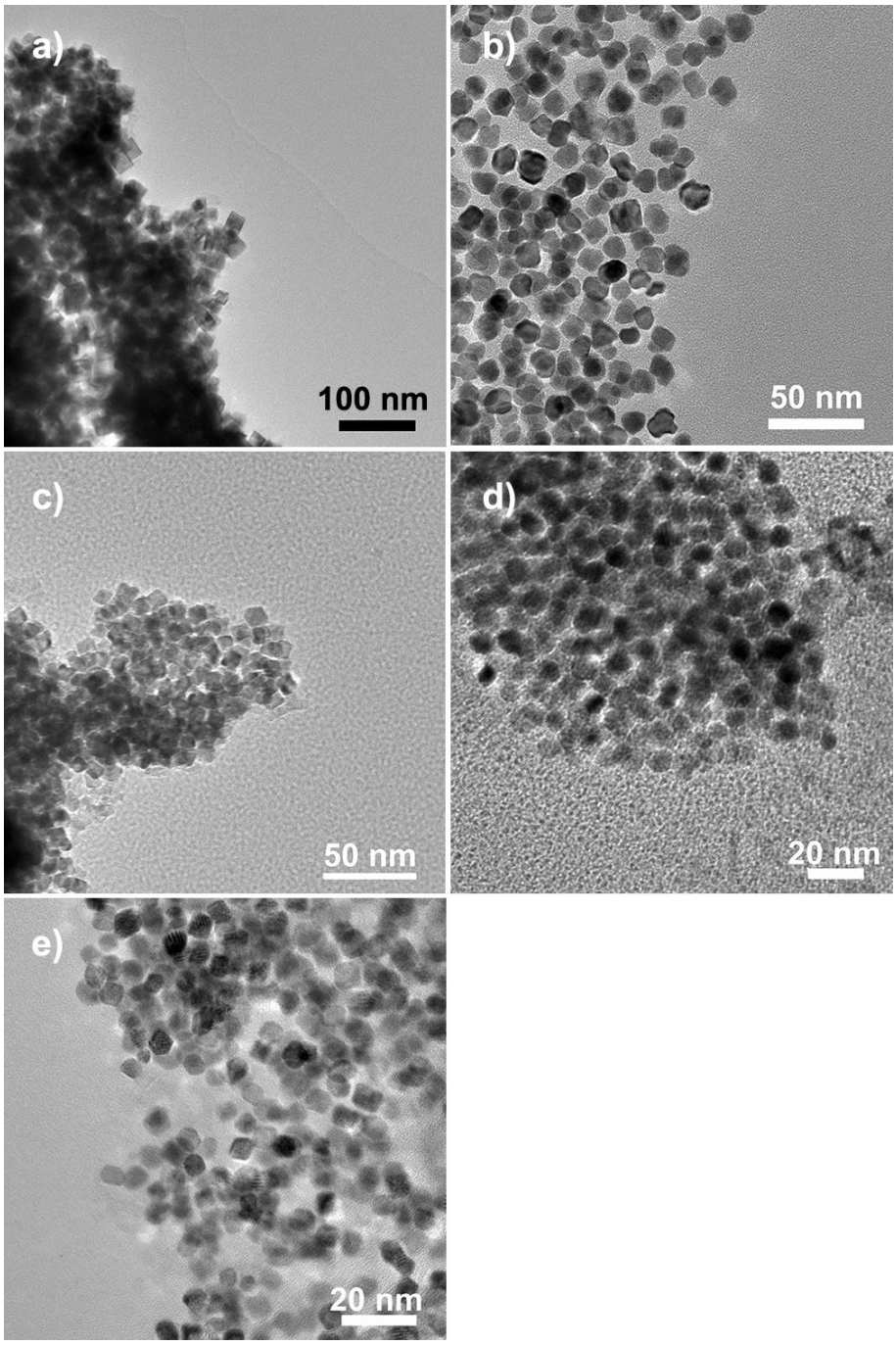

Figure S15. TEM images of shaped Pt−Pd−Rh nanocrystals after electro-chemical tests: a) PtPdRh NCs; b) Pt_3PdRh NCs; c) PtPdRh NTOs; d) $PtPd_3Rh$ NTOs; and e) Pt_3PdRh NTOs.

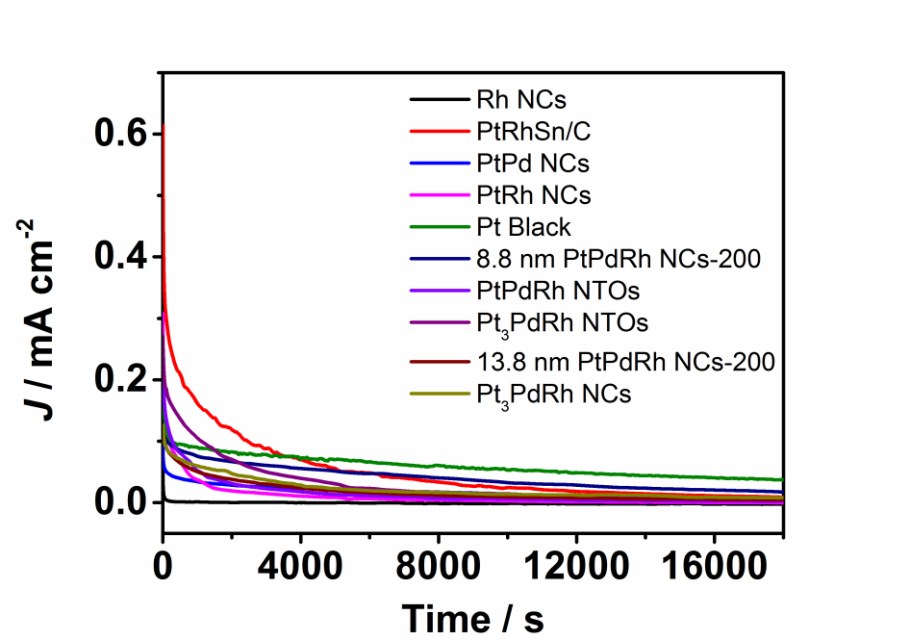

Figure S16. 5 hours' chronoamperometric curves of selected Pt−Pd−Rh NPs at 0.7 V vs. NHE in 0.5 M CH_3CH_2OH/0.1 M $HClO_4$ solution.

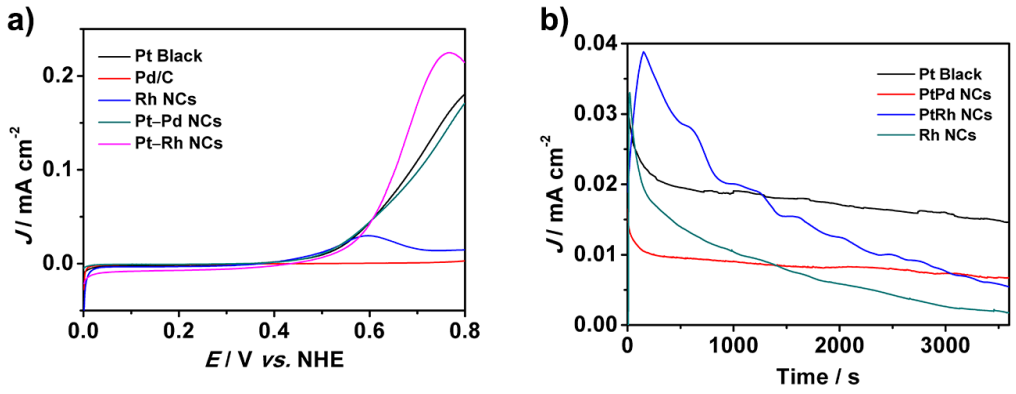

Figure S17. a) LSVs curves and b) chronoamperometric curves recorded at 0.5 V *vs.* NHE of monometallic and bimetallic nanocrystals. The curves of Pt black are added as references.

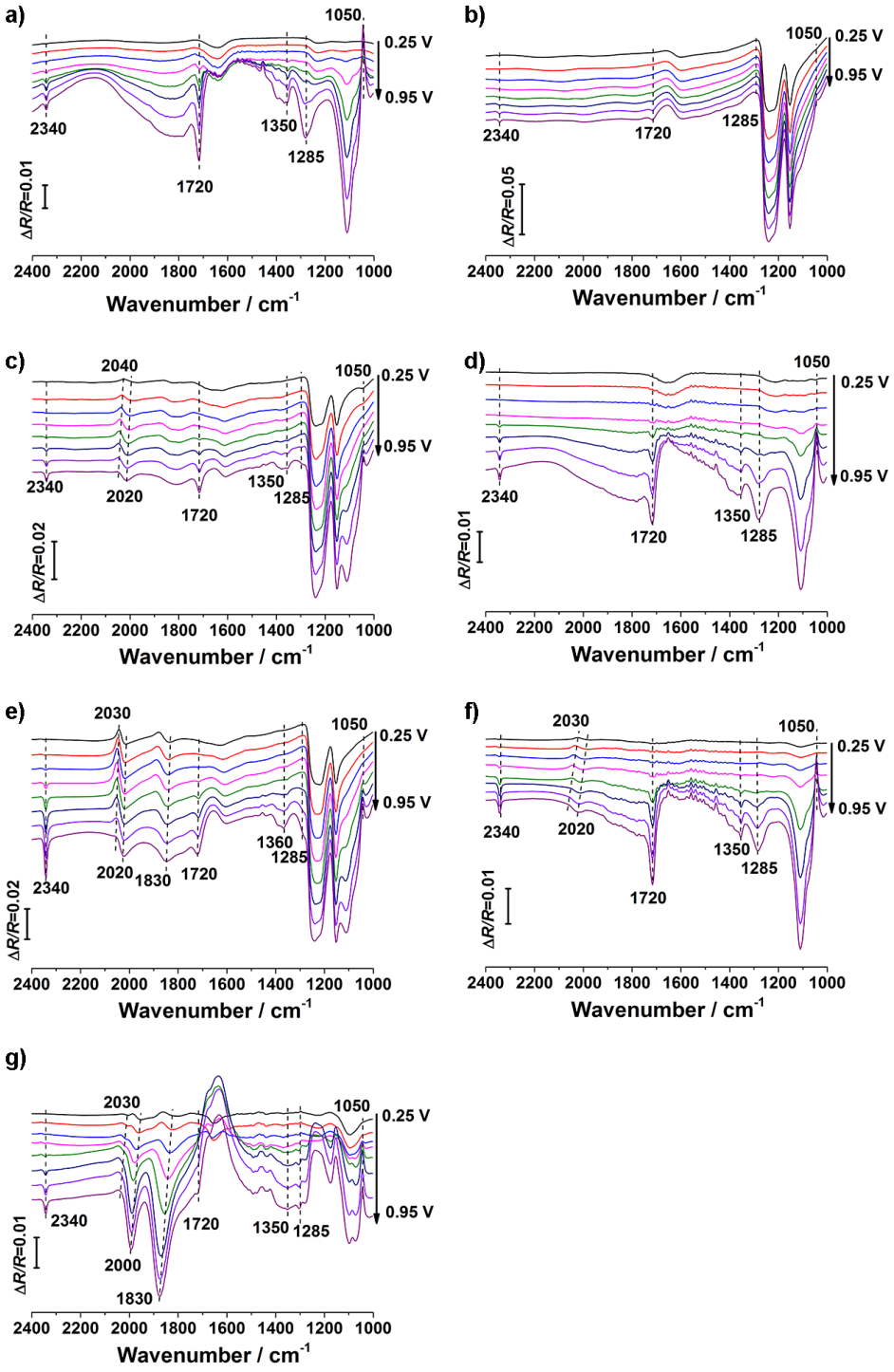

Figure S18. *In situ* EC-FTIR spectra of (a) Pt Black, (b) PtPdRh NCs, (c) Pt_3PdRh NCs, (d) PtPdRh NCs-200, (e) PtPdRh NTOs, (f) Pt_3PdRh NTOs, and (g) $PtPd_3Rh$ NTOs in a mixture of 0.5 M ethanol and 0.1 M $HClO_4$ under a continuous stepped potentials from 0.25 V to 0.95 V. The step of the potential applied is 0.1 V.

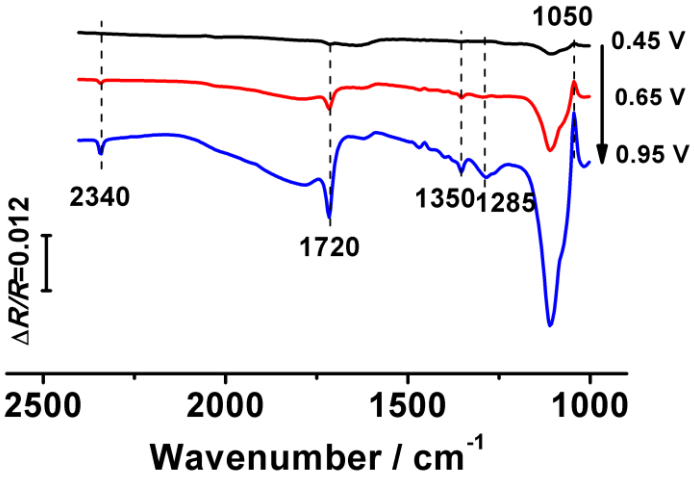

Figure S19. *In situ* FTIR spectra of commercial Pt black at different potentials in a mixture of 0.5 M ethanol and 0.1 M $HClO_4$.

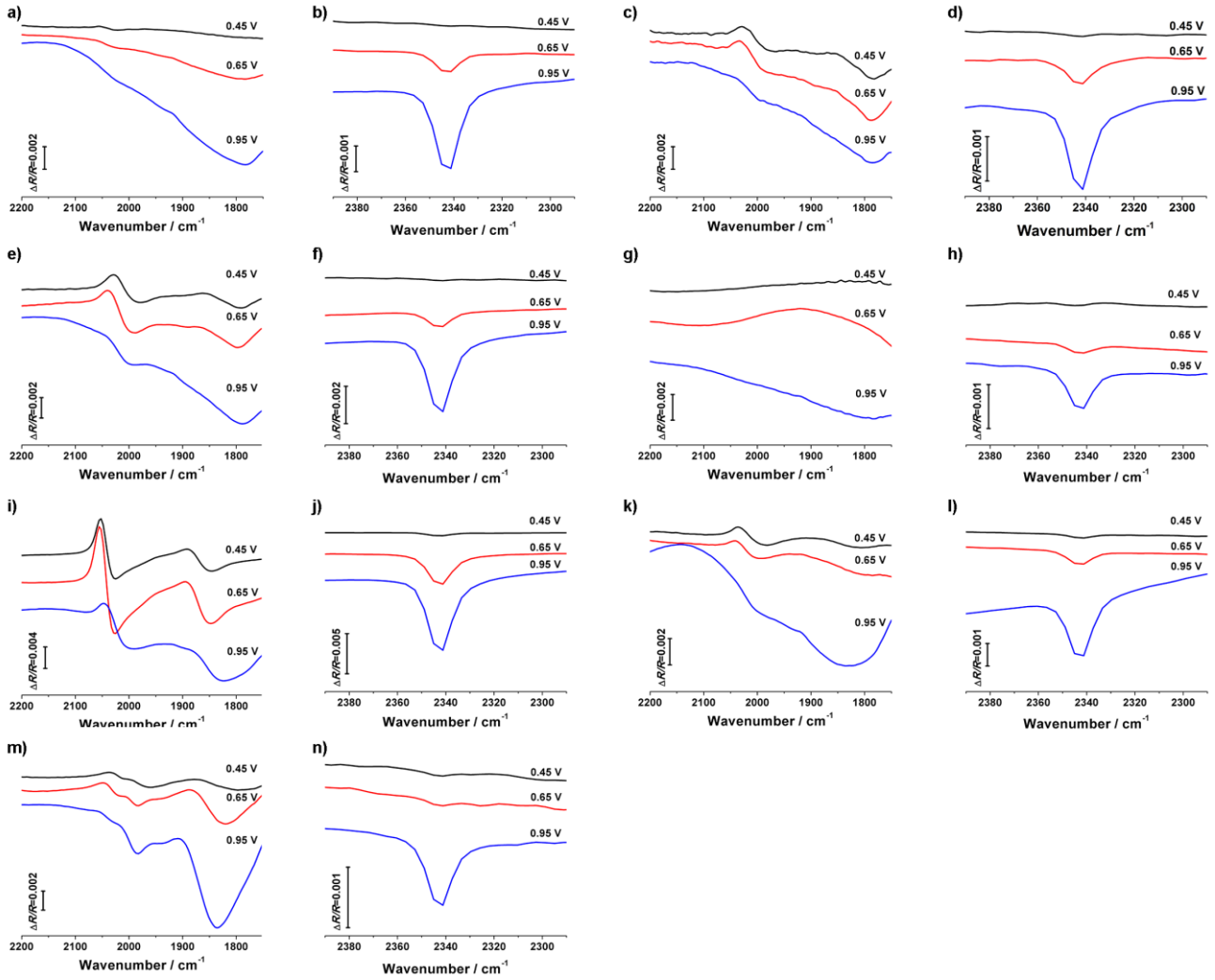

Figure S20. Magnified *in situ* EC-FTIR spectra (Figure 5 in text) in a mixture of 0.5 M ethanol and 0.1 M $HClO_4$ at 0.45 V, 0.65 V, and 0.95 V. The former spectra in each graph were the magnified CO_{ad} part (from 2200 cm^{-1} to 1730 cm^{-1}), and the latter spectra were the magnified CO_2 part (from 2390 cm^{-1} to 2290 cm^{-1}). ((a) and (b) for Pt Black; (c) and (d) for PtPdRh NCs; (e) and (f) for Pt_3PdRh NCs; (g) and (h) for PtPdRh NCs-200; (i) and (j) for PtPdRh NTOs; (k) and (l) for Pt_3PdRh NTOs; (m) and (n) for $PtPd_3Rh$ NTOs)

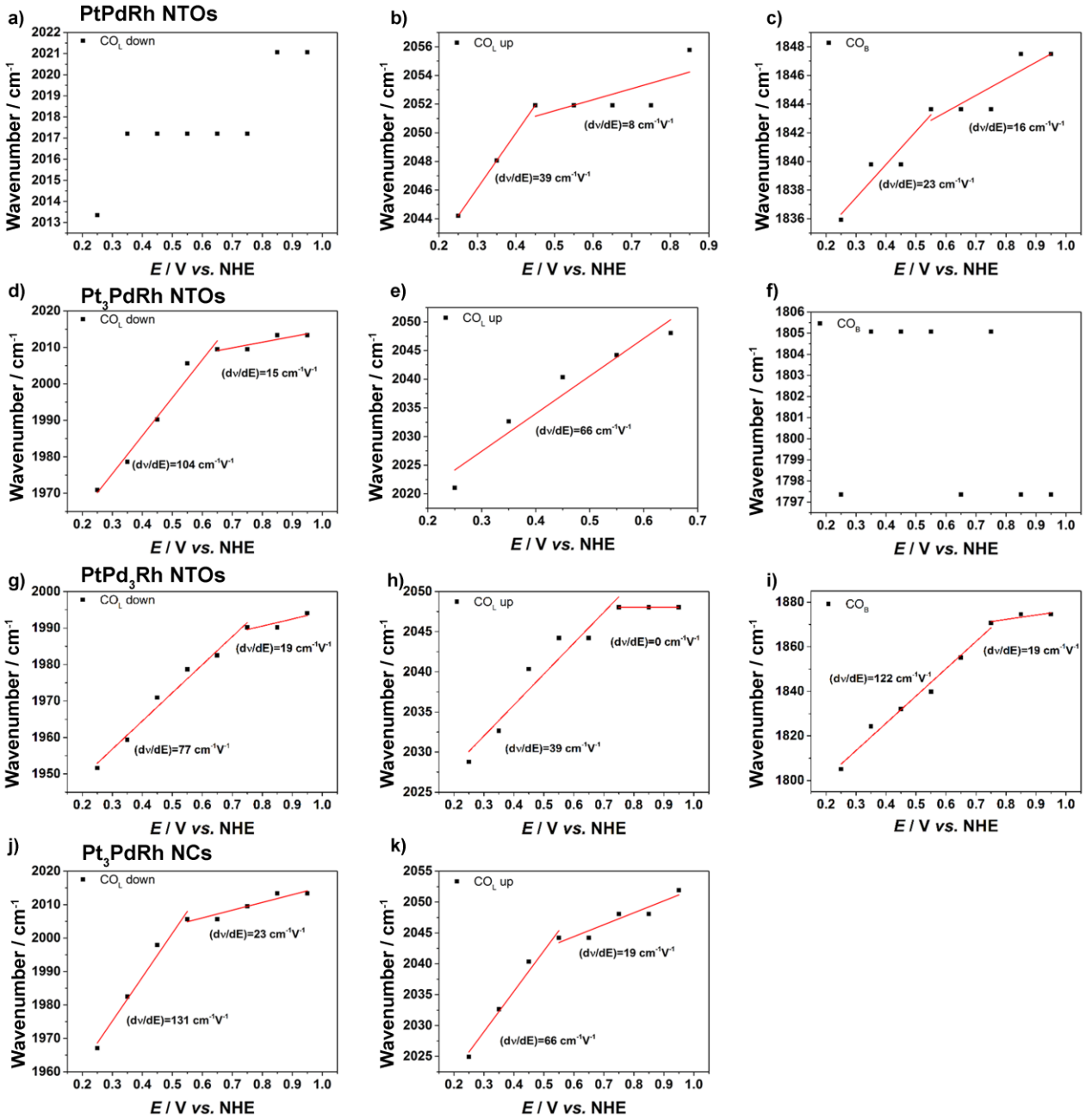

Figure S21. The potential dependence of the band centre frequency for linearly bonded CO (CO_L up and CO_L down) and bridge bonded CO (CO_B) on (a-c) PtPdRh NTOs, (d-f) Pt_3PdRh NTOs, (g-i) $PtPd_3Rh$ NTOs, and (j, k) Pt_3PdRh NCs. (dv/dE) values were the slopes of corresponding fitting lines.

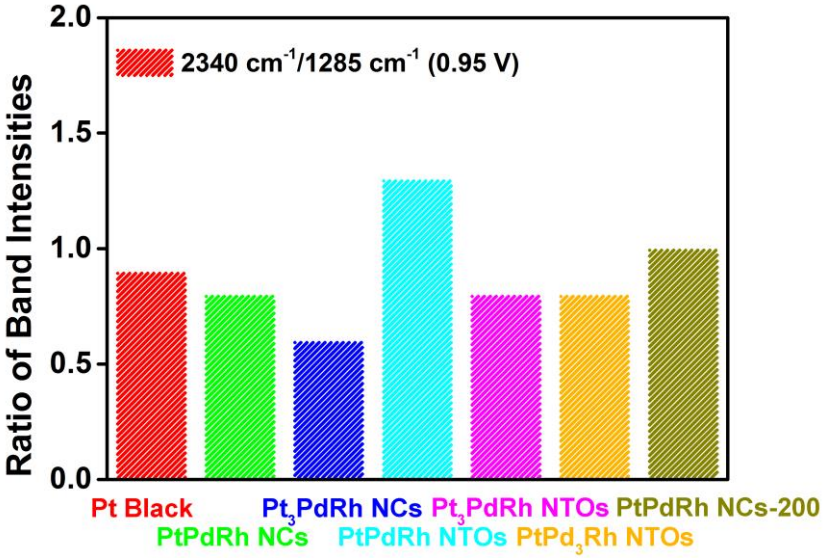

Figure S22. The ratios of in situ FTIR adsorption band intensities of CO_2 at 2340 cm^{-1} to that of acetic acid at 1285 cm^{-1} at 0.95 V.

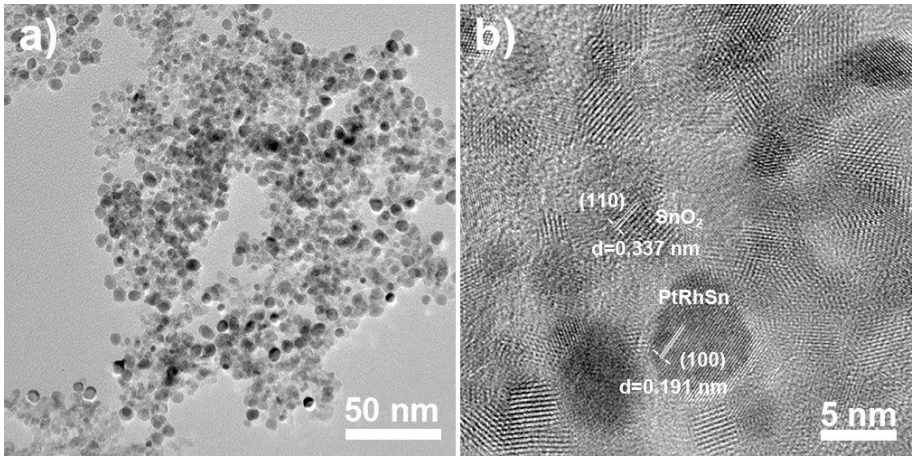

Figure S23. a) TEM and b) HRTEM images of Pt−Rh−Sn NPs prepared by similar hydrothermal method.

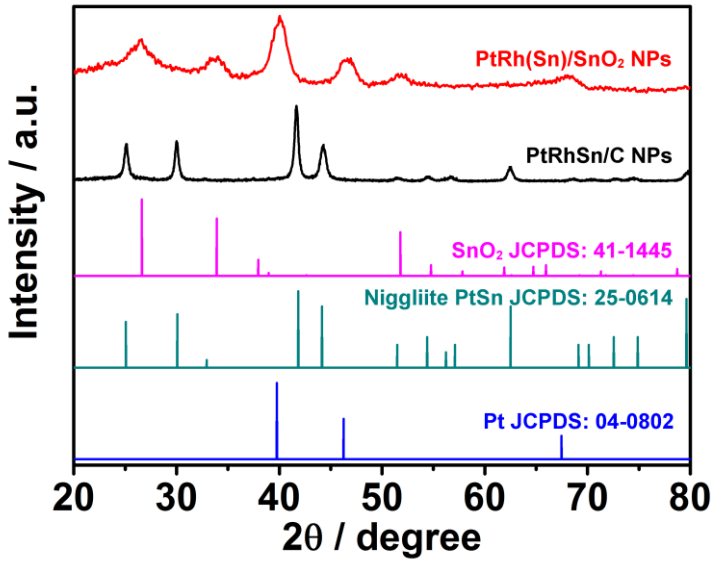

Figure S24. XRD patterns of Pt−Rh−Sn NPs and Pt−Rh−Sn/C NPs synthesized by hydrothermal method and reported solvothermal method.

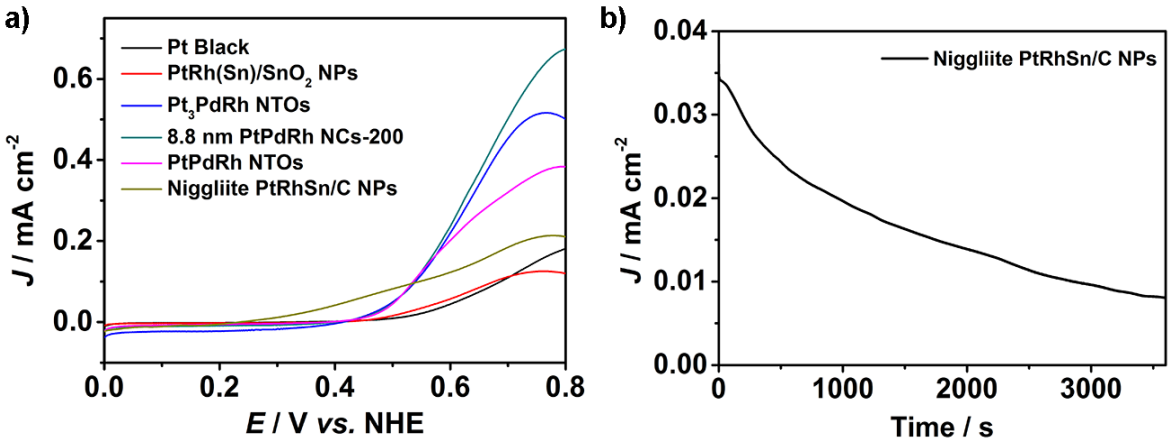

Figure S25. a) LSVs curves and b) chronoamperometric curve recorded at 0.5 V *vs.* NHE of Pt−Rh−Sn NPs. The LSVs curves of Pt black and the Pt−Pd−Rh NPs are added as references.

References

Ref. S1. Powell, C. J.; Jablonski, A. *NIST Electron Inelastic-Mean-Free-Path Database*, 1.2 ed.; National Institute of Standards and Technology, Gaithersburg, MD, **2010**.

Ref. S2. Shao, M.; Adzic, R. R. *Electrochim. Acta* **2005**, *50*, 2415-2422.

Ref. S3. Li, M.; Zhou, W. P.; Marinkovic, N.; Sasaki, K.; Adzic, R. *Electrochim. Acta* **2013**, *104*, 454-461.

Ref. S4. Beyhan, S.; Léger, J.-M.; Kadırgan, F. *Appl. Catal. B-Environ.* **2014**, *144*, 66-74.

Ref. S5. Sun, S.-G.; Yang, D.-F.; Tian, Z.-W. *J. Electroanal. Chem.* **1990**, *289*, 177-187.